

CHEMISTRY

A European Journal

A Journal of



Accepted Article

Title: Structural phase transitions and dielectric switchings in a series of organic-inorganic hybrid perovskites ABX₃ (X = ClO₄⁻ or BF₄⁻)

Authors: Yu-Ling Sun, Xiang-Bin Han, and Wen Zhang

This manuscript has been accepted after peer review and appears as an Accepted Article online prior to editing, proofing, and formal publication of the final Version of Record (VoR). This work is currently citable by using the Digital Object Identifier (DOI) given below. The VoR will be published online in Early View as soon as possible and may be different to this Accepted Article as a result of editing. Readers should obtain the VoR from the journal website shown below when it is published to ensure accuracy of information. The authors are responsible for the content of this Accepted Article.

To be cited as: *Chem. Eur. J.* 10.1002/chem.201702228

Link to VoR: <http://dx.doi.org/10.1002/chem.201702228>

Supported by
ACES

WILEY-VCH

Structural phase transitions and dielectric switchings in a series of organic-inorganic hybrid perovskites ABX_3 ($X = ClO_4^-$ or BF_4^-)

Yu-Ling Sun, Xiang-Bin Han and Wen Zhang*^[a]

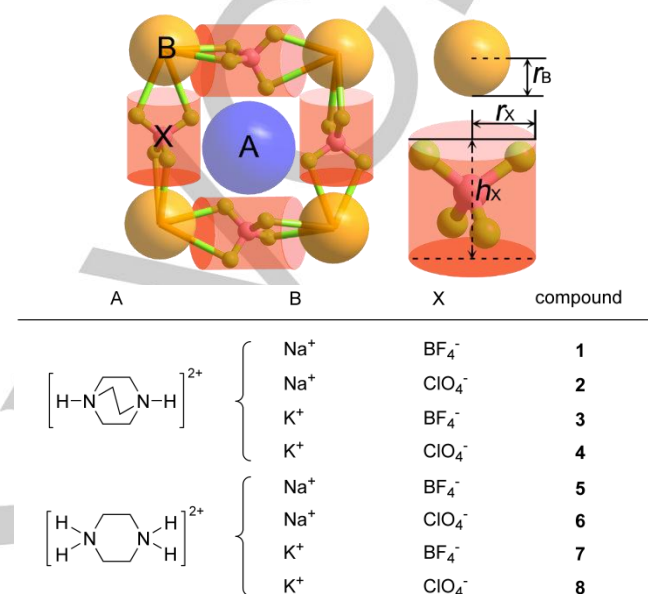
Abstract: A series of organic-inorganic hybrid perovskites ABX_3 (A = diprotonated 1,4-diazabicyclo[2.2.2]octane or piperazine; $B = Na^+$ or K^+ ; $X = ClO_4^-$ or BF_4^-) has been synthesized. They are featured by cubic cage-like host-guest structures of which the A is the cationic guest residing in the anionic cage B_8X_{12} , B is the vertex of the cage with variable coordination numbers between six and twelve, and X is the bridging ligand with mono- and/or bi-dentate coordination modes. Extended Goldschmidt tolerance factor t is used to describe the phase stability of the compounds. Differential scanning calorimetry, variable-temperature structural analyses and dielectric measurements reveal that order-disorder transitions of the A guest and/or X bridging ligand are supposed to be responsible for structural phase transitions and dielectric switchings in the compounds.

Introduction

Perovskite structure is one of the important structures in solid-state materials, showing excellent physical and chemical properties such as magnetism, conductivity, dielectricity, photovoltaics and catalysis.^[1-4] The prototype of perovskite ABX_3 is $CaTiO_3$ whose structure is characterized by octahedrally coordinated $Ti(IV)$ ion and a cage defined by 12 oxygen ions where the $Ca(II)$ ion is located. Extension of the inorganic perovskites to such as two-dimensional perovskites and organic-inorganic hybrid perovskites has greatly enriched the family of this structure.^[5-12] In organic-inorganic hybrid perovskites, the A site is generally replaced by organic components and the X site is changed to bridging ligand such as halide ion, $HCOO^-$, CN^- , N_3^- and so on, forming cubic cage (B_8X_{12}) like host-guest structures. These modifications of the perovskite structure are important and fundamental for screening new materials with desirable properties and functions.

Recent development in molecule-based ferroelectrics and dielectrics shows that the hybrid perovskite structures can play a main role to generate ferroelectric and switchable dielectric properties.^[12,13] It has been found that, generally, origins of the ferroelectric and dielectric transitions are microscopically related with order-disorder transitions of the A guests trapped in the host cages. The dynamic changes of the guest usually trigger structural phase transitions of the perovskites.^[8-10,12] These hybrid perovskites provide good models to investigate the

interplays of interactions between the guest and host that determine the phase stabilities and phase transition-related properties.^[1-4]



Scheme 1. Schematic illustrations of the cubic phase ([100] orientation) and compositions of organic-inorganic hybrid perovskites ABX_3 ($X = ClO_4^-$ or BF_4^-).

Although many types of perovskites have been found, the desire for new structures and properties drives continuous investigations for new types of perovskites. Herein, we report the introduction of ClO_4^- and BF_4^- as the X bridging ligand to construct a new series of organic-inorganic hybrid perovskites. Different from the commonly used monodentate bridging ligands the coordination modes of ClO_4^- and BF_4^- ligands vary between monodentate and chelating when bridging with the B ion which can show the coordination number up to twelve. A series of ABX_3 (A = diprotonated 1,4-diazabicyclo[2.2.2]octane (H_2dabco) or piperazine (H_2pz); $B = Na^+$ or K^+ ; $X = ClO_4^-$ or BF_4^-) has been synthesized and characterized (Scheme 1). Extended Goldschmidt tolerance factor is used to describe the phase stability of the compounds. Most of the compounds in this type show structural phase transitions and dielectric switchings.

Results and Discussion

Synthesis and thermal analysis

Compounds **2–6** were obtained as crystalline samples from aqueous solutions. Phase purities of the samples were confirmed by powder X-ray diffraction (PXRD) measurements (Figure S1). Thermogravimetric analysis (TGA) curves of the crystalline samples of **2**, **3**, **5** and **6** indicate that they remain

[a] Yu-Ling Sun, Xiang-Bin Han, Prof. Wen Zhang
Ordered Matter Science Research Center
College of Chemistry and Chemical Engineering
Southeast University
Nanjing 211189 (China)
E-mail: zhangwen@seu.edu.cn
Supporting information for this article is given via a link at the end of the document

stable below 490 K (Figure S2). Compound **4** was previously reported (Table S1).^[14] Compound **1**, **7** and **8** were not obtained by using the same method as **2–6**.

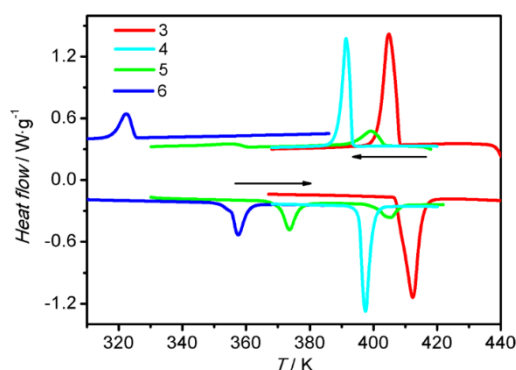


Figure 1. DSC curves of **3–6** measured from 310 K to 440 K.

Table 1. Enthalpy and entropy changes in **3–6**. The microscopic state change N is estimated by using the Boltzmann equation $\Delta S = R \ln N$.

	3	4	5 (T_{tr1} / T_{tr2})	6
ΔH (KJ·mol ⁻¹)	11.92	10.28	4.74 / 3.12	3.32
ΔS (J·mol ⁻¹ ·K ⁻¹)	28.94	25.83	12.67 / 7.71	9.28
N	32.5	22.3	4.6 / 2.5	3.1

Phase transitions in **2–6** were checked by Differential scanning calorimetry (DSC) measurement (Figure 1 and S3). Exception for **2**, the other four undergo reversible phase transitions with endo/exothermic peaks at 412/405 K for **3**, 398/391 K for **4**, 374/353 K (T_{tr1}) and 405/399 K (T_{tr2}) for **5**, and 358/322 K for **6**, upon heating/cooling. The corresponding thermal hystereses of **3–6** are 7 K, 7 K, 21 K (T_{tr1}) and 6 K (T_{tr2}), and 36 K, respectively, at a scanning rate of 10 K min⁻¹. Comparing **3** and **4** or **5** and **6**, it can be found that the phase transition temperatures of the tetrafluoroborates are higher than

Table 2. Crystal data and structure refinements for **2**, **3**, **5** and **6**.

Compound	2	3	5	6	6
T [K]	293	293	293	293	378
Formula	C ₆ H ₁₄ N ₂ NaCl ₃ O ₁₂	C ₆ H ₁₄ N ₂ KB ₃ F ₁₂	C ₄ H ₁₂ N ₂ NaB ₃ F ₁₂	C ₄ H ₁₂ N ₂ NaCl ₃ O ₁₂	C ₄ H ₁₂ N ₂ NaCl ₃ O ₁₂
M_w	435.53	413.72	371.58	409.50	409.50
Crystal system	cubic	cubic	tetragonal	monoclinic	monoclinic
Space group	$Pa-3$	$Pa-3$	$P4_3$	$P2_1/c$	$P2_1/c$
a [Å]	14.198(3)	14.079(2)	9.833(1)	10.170(7)	10.177(7)
b [Å]	14.198(3)	14.079(2)	9.833(1)	9.732(6)	9.750(7)
c [Å]	14.198(3)	14.079(2)	25.908(5)	13.296(9)	13.460(10)
α [°]	90	90	90	90	90
β [°]	90	90	90	92.02(1)	92.11(2)
γ [°]	90	90	90	90	90
V [Å ³]	2862(2)	2790(1)	2505.1(9)	1315(2)	1335(2)
Z	4	8	4	4	4
ρ_{calcd} [g cm ⁻³]	2.022	1.970	1.970	2.068	2.038
μ [mm ⁻¹]	0.743	0.517	0.270	0.801	0.789
Refls. collected / unique	27589 / 1097	18096 / 1075	17066 / 5694	9151 / 3004	9328 / 3048
R_{int}	0.052	0.046	0.082	0.0277	0.0294
$R_1^{[a]}$, $wR_2^{[b]}$ ($I > 2\sigma(I)$)	0.0519, 0.0953	0.0411, 0.1227	0.0661, 0.1462	0.0417, 0.1135	0.0489, 0.1354
$R_1^{[a]}$, $wR_2^{[b]}$ (all data)	0.0574, 0.0972	0.0526, 0.0865	0.1414, 0.1773	0.0524, 0.1200	0.0646, 0.1459
GOF	1.323	1.315	1.032	1.102	1.098
$\Delta\rho^{[c]}$ [e·Å ⁻³]	0.33 / -0.28	0.23 / -0.24	0.35 / -0.22	0.63 / -0.39	0.42 / -0.38

[a] $R_1 = \sum ||F_o| - |F_c|| / |F_o|$. [b] $wR_2 = [\sum w(F_o^2 - F_c^2)^2] / \sum w(F_o^2)^{1/2}$. [c] Maximum and minimum residual electron density.

the corresponding perchlorates. The associated enthalpy changes (ΔH) and entropy changes (ΔS) in the heating process are shown in Table 1, showing an order-disorder type of the phase transitions in these compounds. In particular, the ΔS and N of **3** and **4** are much larger (nearly tenfold) than those of **5** and **6**, indicating different origins of the phase transitions.

It is noteworthy that the phase transition at T_{tr1} in **5** is of thermal history dependence (Figure S3b). During sequential heating-cooling cycles by setting the upper temperature limit being of 393 K in the first cycle and 423 K in the following cycles, the exothermic peaks transform into step-like anomalies and the endothermic peak exhibits downward shift of 2–3 K in each cycle. This phenomenon has been found in a few of phase transition compounds such as some ammonium magnesium-formate frameworks.^[15] The behavior may reflect the case of meta-stable transition.

Crystal structures

Variable-temperature X-ray diffraction analysis was performed on **2–6** to obtain the structures below, between and above the phase transition temperatures (T_{tr}), labelled as room-, intermediate- and high-temperature phases (RTP, ITP and HTP) (Table 2). The structures of **2–6** are featured by similar perovskite structures with metal nodes and BF₄⁻ or ClO₄⁻ linkers to form cubic cages in which the A-site cation (H₂dabco or H₂Pz) resides.

In the RTP at 293 K, crystals **2–4** all crystallize in the cubic system (space group $Pa-3$). With the increases of the sizes of the B ions and X anions, the a , b , c and V values increase a little. The cage volume, calculated by PLATON,^[16] increases in the sequence of 122.26 Å³ (**2**), 124.2 Å³ (**3**) and 125.7 Å³ (**4**). The values of metal–oxygen/fluorine (B–O/F) and metal–metal (B···B) distances are shown in Figure S4 and Table S2. Although the three compounds display different B–O/F distances for their distinct metal coordination modes, the change of the B···B distances is small with a difference of only about 0.06 Å.

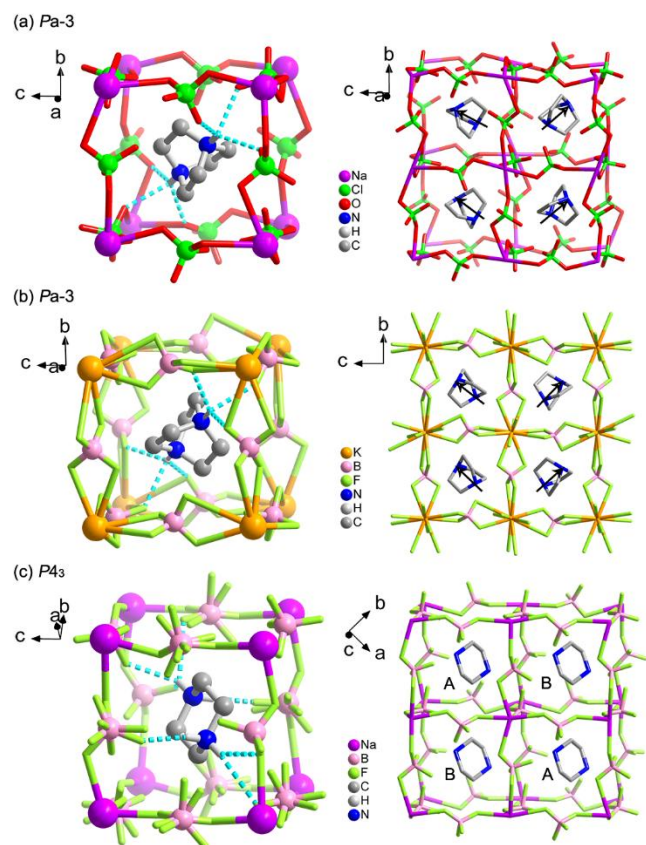


Figure 2. Cage and packing structures of (a) **2**, (b) **3** and (c) **5** at 293 K. The arrows represent the orientations of the A cations in the cages. In (c), the A and B mark two inequivalent guest cations. Dotted lines represent H-bonds. Methylene H atoms are omitted for clarity.

In the host cages, the K^+ ions in **3** and **4** are dodecahedrally coordinated by six BF_4^- ligands and six ClO_4^- ligands, respectively, in a bidentate mode. However, in **2**, the Na^+ ion is hexahedrally coordinated by six ClO_4^- ligands in a monodentate mode. The H_2dabco cations in **2–4** reside in the cages and show a completely ordered state at 293 K. The N...N axis of the cation orients along the body diagonal direction of the cage (C_3 symmetry) (Figure 2a, b and Figure S5). The $-NH$ group of the cation develops trifurcate H-bonds with the X linkers in the host framework. There are two donor-acceptor distances, i.e., 2.980(4) and 3.012(4) Å in **2**, 2.986(3) and 2.975(3) Å in **3**, and 3.079(3) and 3.087(3) Å in **4** (Table S3).

For **5** and **6**, they crystallize in the tetragonal system (space group $P4_3$) and monoclinic system (space group $P2_1/c$), respectively, showing lower symmetries than **2–4**. The asymmetric unit of **5** contains two inequivalent H_2pz cations, two Na^+ ions, and six BF_4^- anions among which four boron atoms (B2, B3, B4, B6) are disordered over two sites. The coordination mode of the Na ions in **5** is the same as those in **2**. In **6**, where the X is ClO_4^- group, all of the components are ordered at 293 K (Figure 3). The metal ion (Na^+) is unique with an octahedral coordination pattern. There are two ClO_4^- groups acting as bidentate ligands along the c axis and the other four acting as

monodentate ligands to bridge two adjacent Na^+ ions. Both **5** and **6** show distorted anionic frameworks with different B–F/O (and B...B) distances (Figure S4, Table S2). The H_2pz cation, exhibiting the similar orientation as H_2dabco , is anchored in the cage by weak H-bonding interactions. The N atoms of the cation are linked to the bridging ligands of the cage through two linear and stronger N–H...F/O hydrogen bonds one bifurcate and one trifurcate weaker H-bonds.

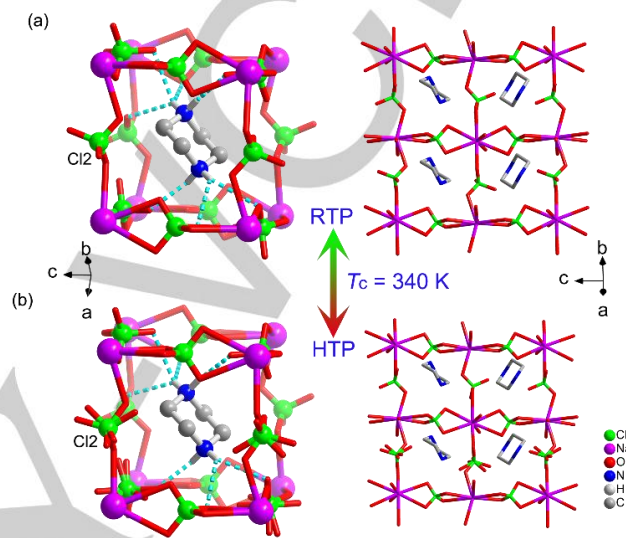


Figure 3. Cage and packing structures of **6** in the (a) RTP and (b) HTP. The ClO_4^- group containing Cl2 is disordered over two sites. Dotted lines represent H-bonds. Methylene H atoms are omitted for clarity.

Although the structures of **2–5** in the RTP are clarified well, their structural information in the ITP and/or HTP have not been obtained due to poor diffraction data. Fortunately, the structure of **6** in the HTP was successfully solved at 378 K. Comparison of the structures of **6** at 378 K and 293 K can help understand the origins of the structure phase transitions in this series of hybrid perovskite compounds. It is noteworthy that both the phases of **6** adopt the same space group with only slight changes of the cell parameters and bond distances and angles (Table 1 and S3). The main structural difference comes from one of the ClO_4^- groups (Cl2) which becomes disordered over two positions in the HTP. The H_2pz cation remains completely ordered during the phase transition. In addition, the B...B distances vary with differences in the range of 0.0145–0.0835 Å and the B...B...B angles show no obvious changes, resulting a slight distortion of the anionic framework (Figure S4). The calculated cavity volume increases from 98.6 Å at 293 K to 102.6 Å at 378 K.

Goldschmidt tolerance factor

For perovskite structures, Goldschmidt tolerance factor (t) can be used to evaluate the stability of the ideal cubic phase ($t = 1$) and the degree of the structural distortion from the cubic phase.^[17] The extended t used for hybrid perovskites was adopted in our case.^[18,19] The anion X is treated as a rigid

cylinder with Shannon effective crystal radius r_X and height h_X (Scheme 1).^[20] The sizes of the ions are calculated by the method reported by Kieslich and Cheetham (Table S4).^[18] The calculated t values of **1–8**, via equation

$$t = (r_A + r_X) / \sqrt{2}(r_B + 0.5h_X)$$

vary between 0.913 and 1.017 (Table 3). For the obtained crystals, the t values are 0.913–0.978 for the cubic **2–4**, 1.017 for the tetragonal **5** and 1.015 for the monoclinic **6**, showing no regular rules for the stability of the cubic phase as shown in other reported hybrid perovskites.^[12e]

Table 3. Calculated tolerance factor t for hybrid perovskite ABX_3 .

Compound	t
1: [H ₂ dabco][Na(BF ₄) ₃]	0.979
2: [H ₂ dabco][Na(ClO ₄) ₃]	0.978
3: [H ₂ dabco][K(BF ₄) ₃]	0.913
4: [H ₂ dabco][K(ClO ₄) ₃]	0.914
5: [H ₂ pz][Na(BF ₄) ₃]	1.017
6: [H ₂ pz][Na(ClO ₄) ₃]	1.015
7: [H ₂ pz][K(BF ₄) ₃]	0.949
8: [H ₂ pz][K(ClO ₄) ₃]	0.949

Dielectric properties

Structural phase transitions can be sensitively detected by dielectric constant ϵ ($\epsilon = \epsilon' - i\epsilon''$, where ϵ' is the real part and ϵ'' the imaginary part) due to local polarization changes.^[21] For **2–6**, the temperature-dependent dielectric constant spectra were measured on powder-pressed pellets (Figure 4 and S6). Except for **2**, **3–6** all show noticeable dielectric transitions at 409 K for **3**, 396 K for **4**, 378 K (T_{tr1}) and 405 K (T_{tr2}) for **5** and 384 K for **6**, consistent with the DSC data. At 1 MHz, **3–6** start with the same ϵ' values of about 5.6 at 310 K and then increase slowly with the increase of temperature in the low-dielectric states. Around the T_{tr} , the values of ϵ' jump into the range of 6.1 and 7.7, corresponding to a dielectric switching behavior. All the dielectric changes show no frequency dependence. It is clear that the dielectric changes around the T_{tr} are much smaller than those reported perovskite structures with striking dielectric transitions, indicating that there are only small polarization changes in the crystals in the HTP.

For **5**, the dielectric curves are measured in the same cycles as the DSC curves (Figure S7). Upon first heating/cooling run below 393 K, the ϵ' curves display an obviously step-like change at T_{tr1} . The second and the third runs below 423 K show

that the dielectric change at T_{tr1} becomes negligible and then shifts to a lower temperature.

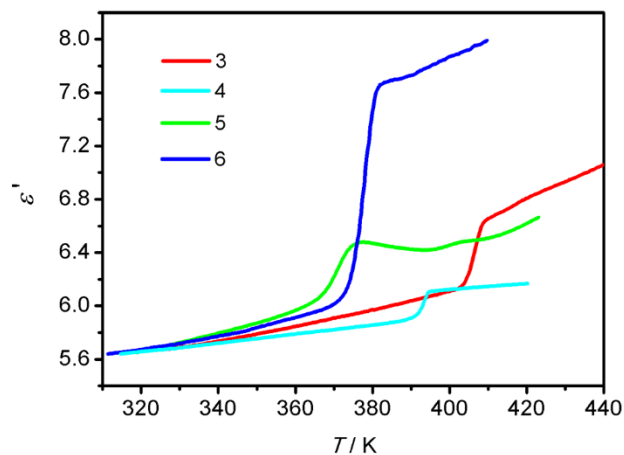


Figure 4. Temperature dependence of the real part of dielectric constant of **3–6** measured at 1 MHz.

Variable-temperature PXRD and IR spectra

Variable-temperature PXRD measurements were performed on **3–6** to further verify the phase transitions (Figure 5 and S8). In the case of **3** and **4**, the patterns at 373 K and 393 K of **3** and 353 K and 398 K of **4** are consistent with those recorded at 293 K, corresponding to the RTP. In the HTP at 423 K, the strength of the diffraction peaks of **3** becomes much weakened while for **4**, the peaks at 25.53°, 28.47°, 33.55° and 35.88° disappear and the left peaks become broad. These findings are ascribed to the structural changes due to the phase transitions, coinciding with the DSC results. For **5**, there are no noticeable changes of the patterns in difference phases, except for the gradual decrease of the peak intensities upon heating. This is similar to **6**, which undergoes an isostructural phase transition with a much smaller entropy change than **3** and **4**.

Temperature dependent IR spectra were also measured on **3–6** in the wavenumber range of 3500–650 cm^{-1} at the selected temperatures above and below the T_{tr} (Figure 6 and S9 and Table S5).^[14a] Taking **5** for example, the spectra show a few changes upon heating. The three peaks at 929, 868 and 773 cm^{-1} , assigned to BF_4^- stretching vibrations, shift downward slightly, indicating changes of the local environment of the bridging ligand. Meanwhile, the bands in the range of 1250–1550 and 2700–3400 cm^{-1} also exhibit obvious changes, which are related to vibrations of H_2pz cations. Upon heating, the weak peaks at 2825 and 3206 cm^{-1} disappear, together with the appearance of new one at 1332 cm^{-1} .^[22] It is noteworthy that the positions of the peaks are more sensitive to the temperature than the intensities. These results prove the structural changes in **3–6**.

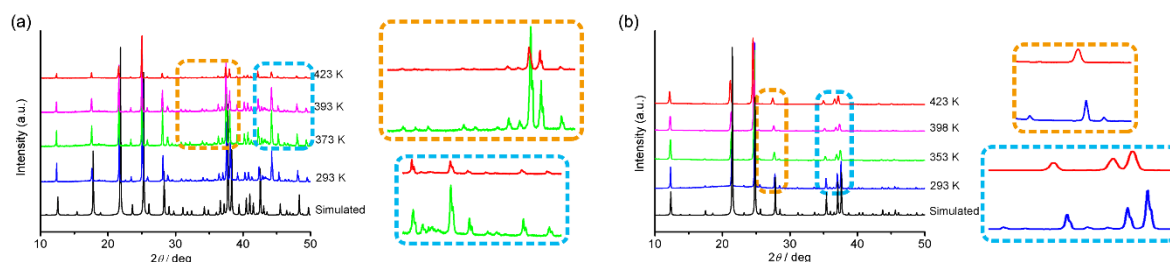


Figure 5. Variable-temperature PXRD patterns of (a) **3** and (b) **4** measured upon heating, together with simulated patterns from single-crystal X-ray diffraction data.

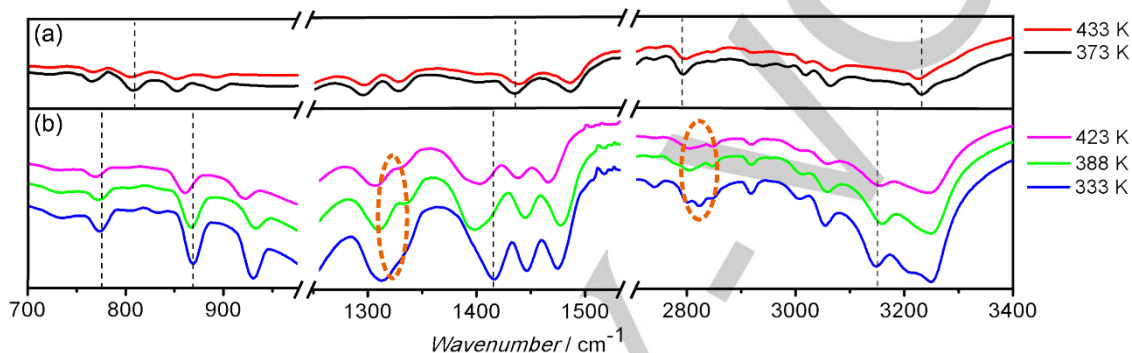


Figure 6. Variable-temperature IR spectra compounds (a) **3** and (b) **5**.

Discussion

Among the series of hybrid perovskites, **1**, **7** and **8** were not obtained as **2–6**. The reason would be ascribed to the weak bonding of the ClO_4^- and BF_4^- to the alkali ions that is sensitive to the components in the aqueous solutions and experimental conditions. It is expected that different equilibrium crystals would be formed besides the hybrid perovskites. For example, not **1** but a new structure in hexagonal system (space group $P-62m$) was found under the same synthetic condition with the cell parameters $a = b = 13.511(2)$ Å, $c = 10.114(2)$ Å and $V = 1598.9(5)$ Å³, which is totally different from the cubic perovskite structures in **2–6**. Unfortunately, this new structure were not successfully solved.

It is noteworthy that the weak interactions between the B and X components also weakens the validity of the calculated t values to predict the stability of the cubic phase of **5** and **6**. As a consequence, the role of the shapes of the A cations on the perovskite structures becomes important. For H_2dabco cation, it has a globular shape (D_{3h}), which naturally follows the concept of Goldschmidt tolerance factor and gives the normal relationship between the t values (0.913–0.978) and the cubic phases of **2–4**. In contrast, the H_2pz cation adopts a chair conformation (D_{3d}) with a more flattened shape than H_2dabco . This drives the phases of **5** and **6** to deviated from the ideal

cubic phases and makes the t values less valid for phase prediction.

It has been known that structural phase transitions in the hybrid perovskites are diverse, which can be caused by tilting and distortions of the anionic octahedra, displacements and/or ordering-disordering of the A and B ions.^[23] For the phase transitions in **3–6**, we can clarify the origins by using the combined experimental results of DSC, X-ray diffraction and dielectric spectra. The origin of the phase transition in **6** is well characterized and ascribed to the order-disorder transition of the ClO_4^- groups of the framework. For **5**, it shows the similar properties to **6** so that it should has the similar origin of the phase transition. However, for **3** and **4**, we suppose a different origin from **5** and **6**. From the DSC results, **3** and **4** show much larger values of the ΔS and N than those of **5** and **6**, indicating the occurrence of order-disorder transitions of the H_2dabco cations that are confined in the cages. This is different from **5** and **6** in which the H_2pz cations are found or supposed to be ordered in both the RTP and HTP. Therefore, in **3** and **4**, the order-disorder transitions of the H_2dabco cations, maybe together with the order-disorder transitions of the B groups, is supposed to account for the phase transitions. Further study is needed to reveal the dynamics of the cations in **3–6**. In addition, the reason that the tetrafluoroborates show higher T_r values than the corresponding perchlorates, such as the pair of **3** and **4**, could be explained on the aspect of internal (chemical pressure) pressure (Table 2 and S1). Considering the smaller size of the BF_4^- than the ClO_4^- , the trapped cation in

tetrafluoroborate **3** would suffer from larger internal pressure imposed by the anionic framework than the counterpart perchlorate **4**, resulting in a relatively higher T_{tr} .

Phase transitions associated with dynamic changes of polar molecules can arouse dielectric transitions between high- and low-dielectric states with relatively large switching ratios.^[12] However, in the series of **1–8**, all the components are centrosymmetric and nonpolar. During the phase transitions, their order-disorder transitions can only contribute small changes of the dielectric constant, resulting in trivial dielectric transitions. To design typical responsive dielectrics with striking dielectric switching, polar A cation should be introduced. This study is now under way.

Conclusions

In summary, a series of hybrid perovskites ABX_3 (A = diprotonated 1,4-diazabicyclo[2.2.2]octane or piperazine; B = Na^+ or K^+ ; X = ClO_4^- or BF_4^-) has been synthesized and characterized. In the anionic B_3X_{12} cage, the vertex B ions exhibit variable coordination numbers between six and twelve and the bridging X ligands adopt mono- and/or chelating coordination modes. Order-disorder transitions of the A guest and/or X bridging ligand are supposed to be responsible for the structural phase transitions and dielectric changes in this series of compounds. This study extends the family of organic-inorganic hybrid perovskites and will prompt investigations of new functional materials.

Experimental Section

Synthesis of **2–6**

Compound **2** was prepared by dissolving dabco, $NaClO_4$ and $HClO_4$ with a molar ratio of 1:1:2 in distilled water. Colorless block-like crystals were harvested after three days at room temperature with slow evaporation of the solution. Compounds **3–6** were prepared in the same way.

2: Yield: 74% based on $NaClO_4$. Elemental analysis calcd (%) for $C_{12}H_{28}N_4Na_2Cl_6O_{24}$ (871.06): C, 16.55; H, 3.24, N, 6.43; found: C, 16.61; H, 3.23; N, 6.55.

3: Yield: 72% based on KBF_4 . Elemental analysis calcd (%) for $C_6H_{14}N_2KB_3F_{12}$ (413.72): C, 17.42; H, 3.41; N, 6.77; found: C, 17.33; H, 3.22; N, 6.69.

4: Yield: 75% based on $KClO_4$. Elemental analysis calcd (%) for $C_6H_{14}N_2KCl_3O_{12}$ (451.64): C, 15.96; H, 3.12, N, 6.20; found: C, 15.98; H, 3.06; N, 6.29.

5: Yield: 76% based on $NaBF_4$. Elemental analysis calcd (%) for $C_8H_{24}N_4Na_2B_6F_{24}$ (743.15): C, 12.93; H, 3.26; N, 7.54; found: C, 12.89; H, 3.15; N, 7.38.

6: Yield: 78% based on $NaClO_4$. Elemental analysis calcd (%) for $C_4H_{12}N_2NaCl_3O_{12}$ (409.5): C, 11.74; H, 2.95; N, 6.84; found: C, 11.81; H, 3.01; N, 6.90.

Materials and measurements

All chemicals were commercially obtained and used without further purification. Variable-temperature IR spectra were measured on a Nicolet6700 spectrometer. TGA was performed on a METTLER TOLEDO STARe System. DSC measurements were carried out on a TA Instruments SDT-Q10 from 300 K to 440 K by a scanning rate of 10 K min^{-1} under nitrogen. PXRD patterns were measured on a Rigaku SmartLab X-ray diffraction instrument. Dielectric constant measurements were performed on a TongHui 2828 impedance analyzer in the frequency range from 1 kHz to 1 MHz under an applied field of 1.0 V in the temperature range 293–440 K.

X-ray Diffraction Experiments

Crystallographic data of **2–6** were collected on a Rigaku Saturn 724⁺ diffractometer by using graphite-monochromated $Mo\ K\alpha$ ($\lambda = 0.71075\ \text{\AA}$) radiation. Data processing was performed using the Crystalclear software package. The structures were solved by direct methods and refined by full-matrix least-square refinements on F^2 by means of the SHELXL-2014 software package. All non-hydrogen atoms were refined anisotropically using all reflections with $I > 2\sigma(I)$. H atoms bonded to N and C atoms were positioned geometrically and refined using a "riding" model with $U_{iso} = 1.2U_{eq}$ (C and N). Details of crystallographic data and structure refinements are listed in Table 1. CCDC 1545911-1545915 contain the supplementary crystallographic data for this paper. These data can be obtained free of charge from The Cambridge Crystallographic Data Centre via www.ccdc.cam.ac.uk/data_request/cif.

Acknowledgements

This work was supported by the NSFC (Grant No. 21225102).

Keywords: perovskites • cage • phase transition • dielectric switching

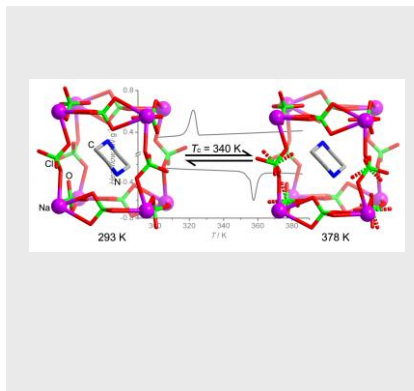
- [1] F. S. Galasso, *Structure, Properties and Preparation of Perovskite Type Compounds*, Pergamon Press, Oxford, **1969**.
- [2] *Properties and Applications of Perovskite Type Oxides* (Eds.: L. J. Tejuca, J. L. G. Fierro), Marcel Dekker, New York, **1993**.
- [3] C. N. R. Rao, B. Raveau, *Colossal Magnetoresistance, Charge Ordering and Related Properties of Manganese Oxides*, World Scientific, Singapore, **1998**.
- [4] A. R. Akbashev, A. R. Kaul, *Russ. Chem. Rev.* **2011**, *80*, 1159–1177.
- [5] D. B. Mitzi, C. A. Feild, W. T. A. Harrison, A. M. Guloy, *Nature* **1994**, *369*, 467–469.
- [6] S. Kazim, M. K. Nazeeruddin, M. Grätzel, S. Ahmad, *Angew. Chem. Int. Ed.* **2014**, *53*, 2812–2824.
- [7] a) B. Kundys, A. Lappas, M. Viret, V. Kapustianyk, V. Rudyk, S. Semak, C. Simon, I. Bakaimi, *Phys. Rev. B* **2010**, *81*, 224434; b) A. O. Polyakov, A. H. Arkenbout, J. Baas, G. R. Blake, A. Meetsma, A. Caretta, P. H. M. van Loosdrecht, T. T. M. Palstra, *Chem. Mater.* **2012**, *24*, 133–139; c) W.-Q. Liao, Y. Zhang, C.-L. Hu, J.-G. Mao, H.-Y. Ye, P.-F. Li, S. D. Huang, R.-G. Xiong, *Nat. Commun.* **2015**, *6*, 7338.
- [8] a) X.-Y. Wang, L. Gan, S.-W. Zhang, S. Gao, *Inorg. Chem.* **2004**, *43*, 4615–4625; b) P. Jain, N. S. Dalal, B. H. Toby, H. W. Kroto, A. K. Cheetham, *J. Am. Chem. Soc.* **2008**, *130*, 10450–10451; c) P. Jain, V.

- Ramachandran, R. J. Clark, H. D. Zhou, B. H. Toby, N. S. Dalal, H. W. Kroto, A. K. Cheetham, *J. Am. Chem. Soc.* **2009**, *131*, 13625–13627; d) S. Chen, R. Shang, K. L. Hu, Z. M. Wang, S. Gao, *Inorg. Chem. Front.* **2014**, *1*, 83–98; e) S. Chen, R. Shang, B.-W. Wang, Z.-M. Wang, S. Gao, *Angew. Chem. Int. Ed.* **2015**, *127*, 11245–11248.
- [9] Q. Pan, Z.-B. Liu, Y.-Y. Tang, P.-F. Li, R.-W. Ma, R.-Y. Wei, Y. Zhang, Y.-M. You, H.-Y. Ye, R.-G. Xiong, *J. Am. Chem. Soc.* **2017**, *139*, 3954–3957.
- [10] a) X.-H. Zhao, X.-C. Huang, S.-L. Zhang, D. Shao, H.-Y. Wei, X.-Y. Wang, *J. Am. Chem. Soc.* **2013**, *135*, 16006–16009; b) Z.-Y. Du, T.-T. Xu, B. Huang, Y.-J. Su, W. Xue, C.-T. He, W.-X. Zhang, X.-M. Chen, *Angew. Chem. Int. Ed.* **2015**, *54*, 914–918.
- [11] D. B. Mitzi, *Prog. Inorg. Chem.* **1999**, *48*, 1–121.
- [12] a) W. Zhang, Y. Cai, R.-G. Xiong, H. Yoshikawa, K. Awaga, *Angew. Chem. Int. Ed.* **2010**, *122*, 6758–6760; b) W. Zhang, H.-Y. Ye, R. Graf, H. W. Spiess, Y.-F. Yao, R.-Q. Zhu, R.-G. Xiong, *J. Am. Chem. Soc.* **2013**, *135*, 5230–5233; c) X. Zhang, X.-D. Shao, S.-C. Li, Y. Cai, Y.-F. Yao, R.-G. Xiong, W. Zhang, *Chem. Commun.* **2015**, *51*, 4568–4571; d) C. Shi, X. Zhang, Y. Cai, Y.-F. Yao, W. Zhang, *Angew. Chem. Int. Ed.* **2015**, *54*, 6206–6210; e) C. Shi, C.-H. Yu, W. Zhang, *Angew. Chem. Int. Ed.* **2016**, *128*, 5892–5896; f) Y.-L. Liu, W. Zhang, *Chem. Commun.* **2017**, *53*, 6077–6080.
- [13] W. Zhang, R.-G. Xiong, *Chem. Rev.* **2012**, *112*, 1163–1195.
- [14] a) Z. M. Jin, Y. J. Pan, X. F. Li, M. L. Hu, L. Shen, *J. Mol. Struct.* **2003**, *660*, 67–72; b) G. Feng, X. Jiang, W. Wei, P. Gong, L. Kang, Z. Li, Y. Li, X. Li, X. Wu, Z. Lin, W. Li, P. Lu, *Dalton Trans.* **2016**, *45*, 4303–4308.
- [15] R. Shang, G. C. Xu, Z. M. Wang, S. Gao, *Chem. Eur. J.* **2014**, *20*, 1146–1158.
- [16] A. L. Spek, *Acta Cryst. D* **2009**, *65*, 148–155.
- [17] V. M. Goldschmidt, *Naturwissenschaften* **1926**, *14*, 477–485.
- [18] a) G. Kieslich, S. Sun, A. K. Cheetham, *Chem. Sci.* **2014**, *5*, 4712–4715; b) G. Kieslich, S. Sun, A. K. Cheetham, *Chem. Sci.* **2015**, *6*, 3430–3433.
- [19] D. B. Mitzi, *J. Chem. Soc. Dalton Trans.* **2001**, *1*, 1–12.
- [20] R. D. Shannon, *Acta Cryst. A* **1976**, *32*, 751–767.
- [21] H. Fröhlich, *Theory of dielectrics (2nd ed.)*, Oxford University Press, Oxford, UK, **1965**.
- [22] a) D. Lin-Vien, N. B. Colthup, W. G. Fateley, J. G. Grasselli, *The Handbook of Infrared and Raman Characteristic Frequencies of Organic Molecules*, Academic Press, San Diego, CA, **1991**; b) M. Wojtaś, A. Gągor, O. Czupiński, W. Medycki, R. Jakubas, *J. Solid State Chem.* **2012**, *187*, 35–44; c) A. M. Petrosyan, *Vibrational Spectroscopy* **2007**, *43*, 284–289; d) M. T. Messina, P. Metrangolo, W. Navarrini, S. Radice, G. Resnati, G. Zerbi, *J. Mol. Struct.* **2000**, *524*, 87–94; e) O. Czupiński, R. Jakubas, A. Pietraszko, *J. Mol. Struct.* **2004**, *704*, 177–187.
- [23] a) A. M. Glazer, *Acta Cryst. B* **1972**, *28*, 3384–3392; b) P. M. Woodward, *Acta Cryst. B* **1997**, *53*, 44–66; c) I. N. Flerov, M. V. Gorev, K. S. Aleksandrov, A. Tressaud, J. Grannec, M. Couzi, *Mater. Sci. & Engin. R* **1998**, *24*, 81–151; d) K. S. Aleksandrov, J. Bartolomé, *Phase Transitions* **2001**, *74*, 255–335; e) M. C. Knapp, P. M. Woodward, *J. Solid State Chem.* **2006**, *179*, 1076–1085; f) G. King, P. M. Woodward *J. Mater. Chem.* **2010**, *20*, 5785–5796.

Entry for the Table of Contents

FULL PAPER

A series of organic-inorganic hybrid perovskites ABX_3 (A = diprotonated 1,4-diazabicyclo[2.2.2]octane or piperazine; B = Na^+ or K^+ ; X = ClO_4^- or BF_4^-) has been synthesized, showing structural phase transitions and dielectric switchings that are caused by order-disorder transitions of the A guest and/or X bridging ligand.



Yu-Ling Sun, Xiang-Bin Han, Wen Zhang*

Page No. – Page No.

Structural phase transitions and dielectric switchings in a series of organic-inorganic hybrid perovskites ABX_3 (X = ClO_4^- or BF_4^-)